



# Root Cause Analysis of Failed AISI 440C High Carbon Stainless Steel Used in Aerospace Actuator Systems

Lagudu Yerrinaidu · K. Jalaja · Sushant K. Manwatkar · Rohit Kumar Gupta

Submitted: 18 April 2024 / Accepted: 21 April 2024 / Published online: 24 May 2024  
© ASM International 2024

**Abstract** AISI 440C is a high carbon martensitic stainless steel with superior wear and abrasion resistance among all grades of stainless steel. Hydraulic amplifier valve (HAV) spools, made of AISI 440C stainless steel, are used in flow control devices of launch vehicle actuator systems. In the present case, a failure occurred near the undercut region of the HAV spool during the vibration test. The failure was observed specifically at M5 threaded region of the spool. A detailed investigation has been carried out to understand the root cause of the failure. 612  $\mu\text{m}$  deep pit was observed with corrosion products on the fracture surface near to the undercut region of M5 thread. Elemental chemical composition analysis via energy-dispersive X-ray spectroscopy (EDS) confirmed the presence of oxygen and chlorine in the pit location. Primary carbides exposed to the rough machined surface at the undercut region lead to the pit initiation and propagation because of the galvanic potential difference between matrix and primary carbides. Failure of the HAV spool is attributed to corrosion-assisted overload.

**Keywords** HAV spool · Actuator · 440C · Primary carbides · Pitting corrosion · Overload

## Introduction

AISI 440 C is a high-carbon martensitic stainless steel with superior wear and abrasion resistance among all the grades of stainless steel. 440C stainless steels are extensively used

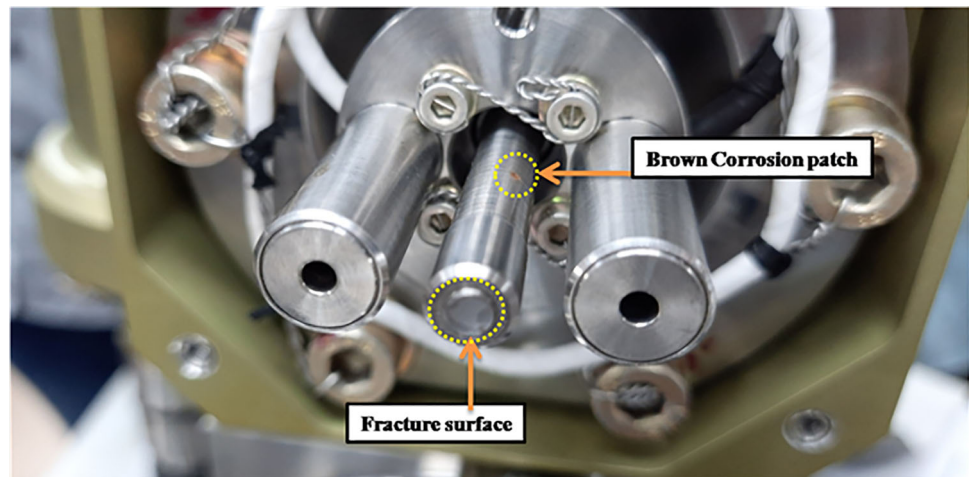
in aerospace for ball bearings and hydraulic control valve assemblies [1–3]. Corrosion resistance is an important consideration for hydraulic valve applications. Even though high carbon content aids the functional needs of the steel, corrosion resistance reduction takes place by the formation of primary and secondary carbides of chromium [4, 6–8]. The chromium content (18wt.%) in AISI 440C steel is equivalent to corrosion resistance of austenitic stainless steel, but its corrosion resistance becomes inferior to austenitic grade due to most of the chromium being shared by carbon; there is no extra chromium to heal the damages in the passivated chromium oxide layer. A minimum of 11 wt.% Cr is required to form the chromium oxide film uniformly; chromium content less than 11wt.% can cause localized damage by forming pits [4, 5]. Pits are formed near  $\text{M}_7\text{C}_3$  primary carbides due to less chromium in the matrix [3]. The presence of more elemental chromium in the martensite matrix will enhance the corrosion resistance by forming the passive chromium oxide layer [9, 10].

Chlorine-rich atmosphere damages the passive layer and subsequently leads to the formation of pits. Hydrolysis at the pit location goes into autocatalytic mode and pits grow further and further until they perforates [4, 11]. Pit size, shape, and depth depend on several factors. Deep narrow pits act as severe stress concentration in loading. In aggressive corrosive environments, 440C steel has very poor corrosion resistance; in such cases, pitting and corrosion become more dynamic. In several conditions, pits act as initiators for stress corrosion cracking (SCC) and crevice corrosions. Austenitizing temperature plays a role in the control of primary carbide content [12]. Austenite treatment at higher temperatures leads to the dissolution of more primary carbides; as a result, matrix is enriched with

---

L. Yerrinaidu (✉) · K. Jalaja · S. K. Manwatkar · R. K. Gupta  
Materials and Mechanical Entity, Vikram Sarabhai Space  
Centre, ISRO, Thiruvananthapuram 695022, India  
e-mail: lagudunaidu3@gmail.com

**Fig. 1** Photograph showing the failed HAV spool with failure location with arrow



elemental carbon. During hardening it will bring down the Ms temperature. As a result, martensite transformation will be incomplete and some fraction of austenite is retained. Austenitizing at lower temperatures decreases the corrosion resistance by retention of more primary carbides; as a result, martensitic matrix depleted with free form of chromium [5, 13]. Considering both these aspects hardening temperature is selected.

Hydraulic amplifier valve (HAV) spools are used in flow control devices of launch vehicle actuator systems. In the current case, failure was observed near the undercut region of the HAV spool during the vibration test (Fig. 1). It failed during the vibration check for use in the flight. A detailed investigation has been carried out to understand the root cause of the failure.

## Experimental

HAV spools are realized through a vacuum arc melting route. Visual and stereomicroscopic observations were carried out on the failed HAV spool. Fractographic analysis was carried out on the fracture surface under Carl Zeiss EV 50 scanning electron microscope (SEM) and chemical composition was analyzed by OXFORDX-Max<sup>N</sup> energy dispersed X-ray spectroscopy (EDS). One of the fracture portions was sectioned vertically with the slow-speed diamond cutting machine for optical metallographic analysis. Emery polishing was done using different grades of emery papers. Final polishing was done using alumina followed by diamond paste. A metallographically prepared sample was observed under an optical microscope. Etching was carried out using 1% Nital for 10 s by swabbing. Etched specimens were observed under Olympus GX 71 optical microscope. Microhardness measurements were carried out by using a Wilson hardness machine with a 300gf load. Further, electron backscattered diffraction analysis (EBSD) was also carried out using a field emission scanning

electron microscope (FESEM) of Carl Zeiss Gemini 560 with a step size of 0.5  $\mu\text{m}$  and voltage of 20 kV. Buehler Vibromet polishing machine was used with 0.05  $\mu\text{m}$  size colloidal silica solution in the final polishing for 24 h to get the clear Kikuchi patterns. Post-processing analysis was done by using Aztec Crystal software.

## Results and Discussion

### Visual, Digital and Stereomicroscopic Observations

Visual and stereomicroscopic observations showed fracture occurred at the undercut region of the M5 thread portion as shown in Fig. 2. Both spool side and screw side fracture surfaces were having corrosion products as shown in Fig. 3a and b. The undercut region of the fracture surface revealed rough machining marks (Fig. 3c). Brown color corrosion patch was observed on the spool surface portion, which is slightly away from the fracture edge (Fig. 3d).

### Scanning electron microscopy (SEM) and Energy Dispersed X-ray Spectroscopy (EDS) analysis

SEM observations on the HAV spool fracture surface revealed corrosion products present near to edge locations (undercut region with rough machine marks). Corrosion pit of approx. 612  $\mu\text{m}$  depth was observed in the fracture location (Fig. 4a, b and c). EDS elemental analysis confirmed the presence of oxygen and chlorine in the pit area (Fig. 5). The fracture surface away from the pit region has dimple features with primary carbide fragmentation in a brittle manner along with spherical secondary carbides (Fig. 6). Rough machine marks and small pits were observed at the undercut region of the fracture edge side (Fig. 7). A corrosion patch was observed on the HAV spool body away from the fracture surface (Fig. 8). SEM&EDS

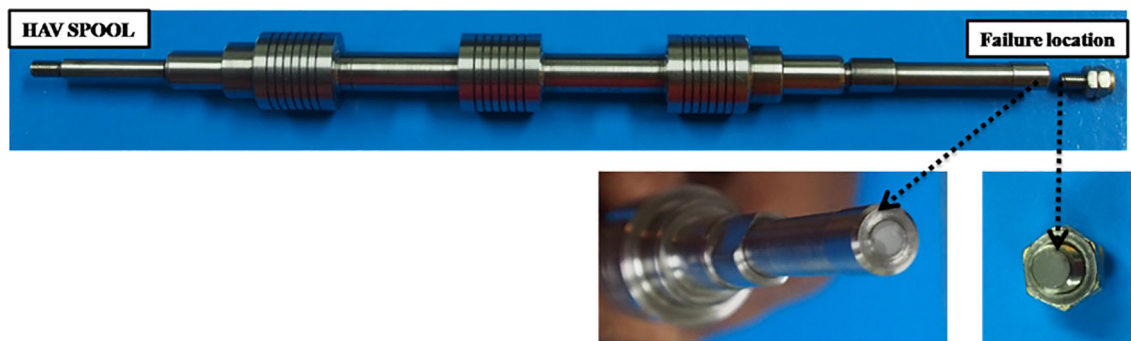


**Fig. 2** Photographs showing fracture surfaces of HAV spool both side and corrosion patch present on the surface

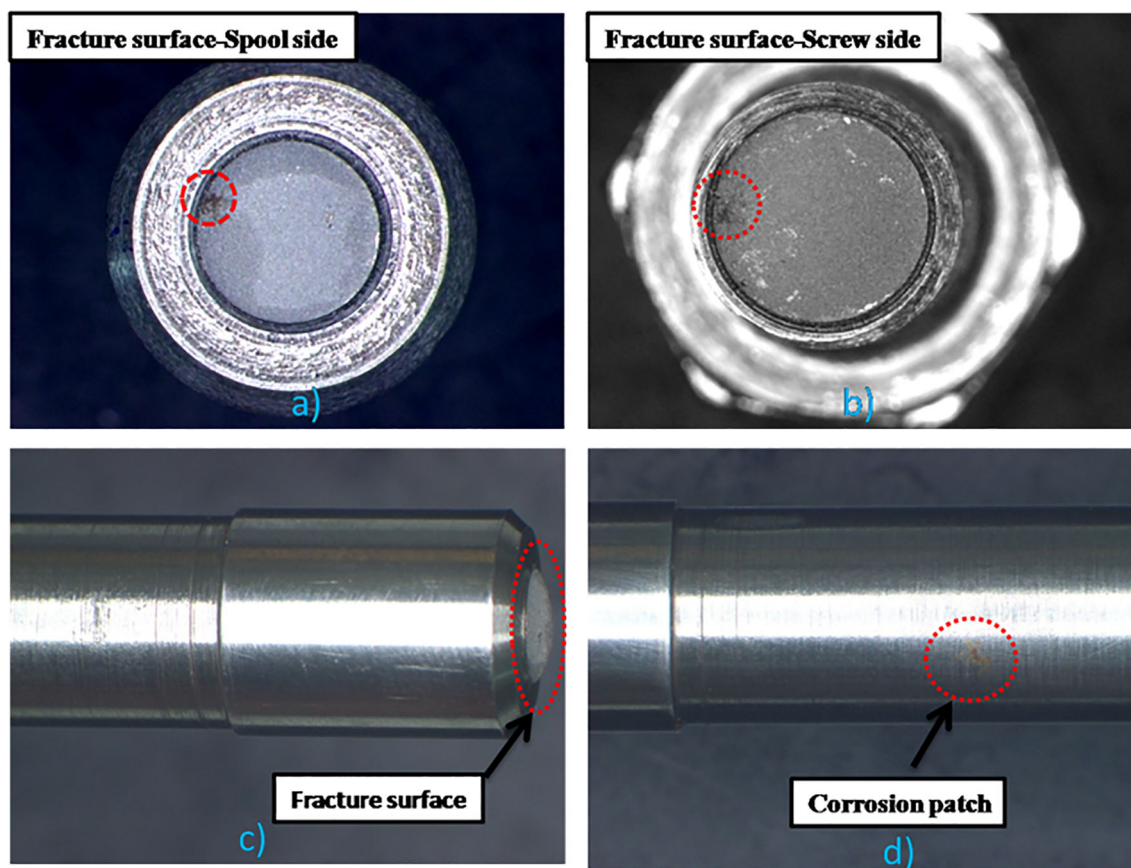


**Fig. 3** Photographs showing fracture surfaces of HAV spool both sides and corrosion patch present on the surface

elemental analysis revealed the pit morphology and chemistry. Oxygen and chlorine presence were confirmed at the pit location in the corrosion patch. Chlorine concentration at the pit location is high as shown in Fig. 9.

SEM micrographs revealed primary and secondary carbides with different sizes and geometry (Fig. 10 a, b, c and d). Primary carbides are in irregular shapes with different sizes-based Cr/Fe ratio. Secondary carbides are in spherical morphology with different sizes, formed during the tempering stage. EDS area map analysis confirmed the chromium-rich phases with high chromium concentration

(Fig. 11). Line scan analysis confirmed the Cr variation at the martensitic matrix and carbides (Fig. 12).

Based on the SEM observations, it is clear that failure has occurred due to a deep pit at the undercut region. During vibration test, this pit acted as a notch and reduced the load-bearing area; hence, fracture occurred at the undercut region. It is well known that primary carbides form during the solidification of the liquid metal. Some of these carbides will be exposed to the surface during the machining stage. The corrosion pits preferentially initiate around the bigger primary carbides due to the potential



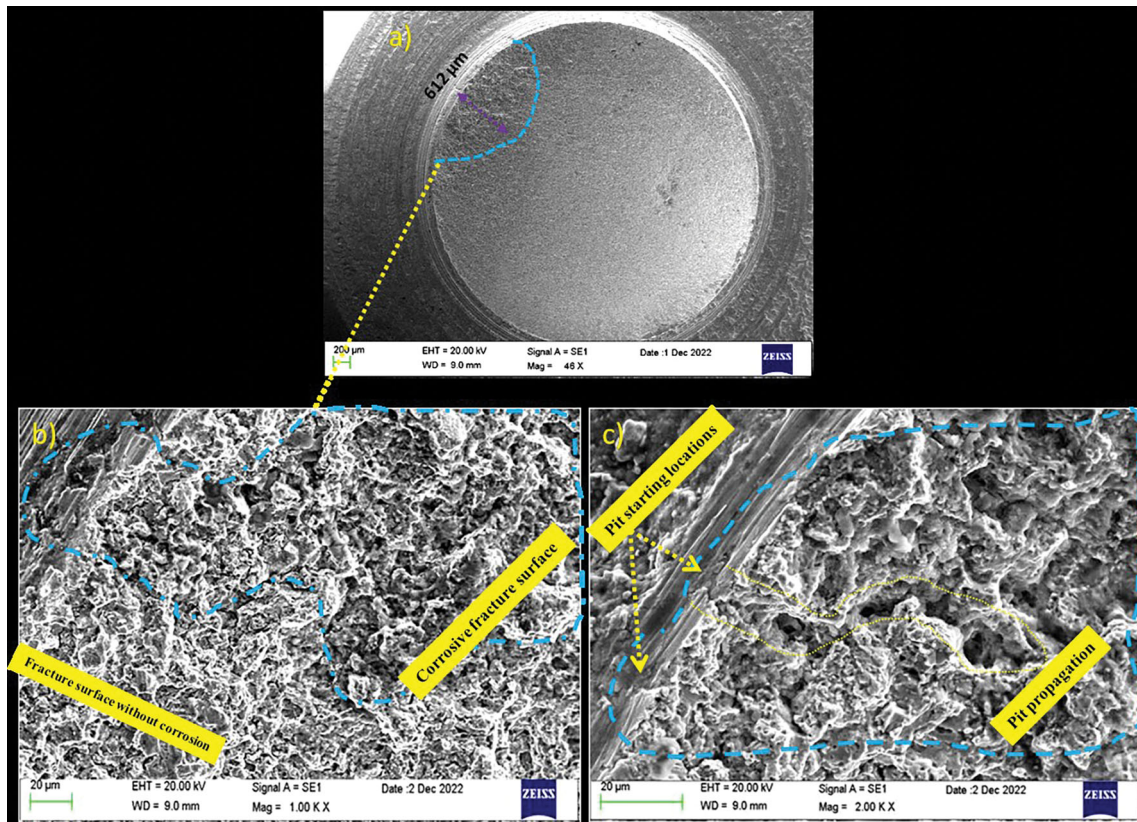


Fig. 4 SEM Fractographs showing the Pit region and away

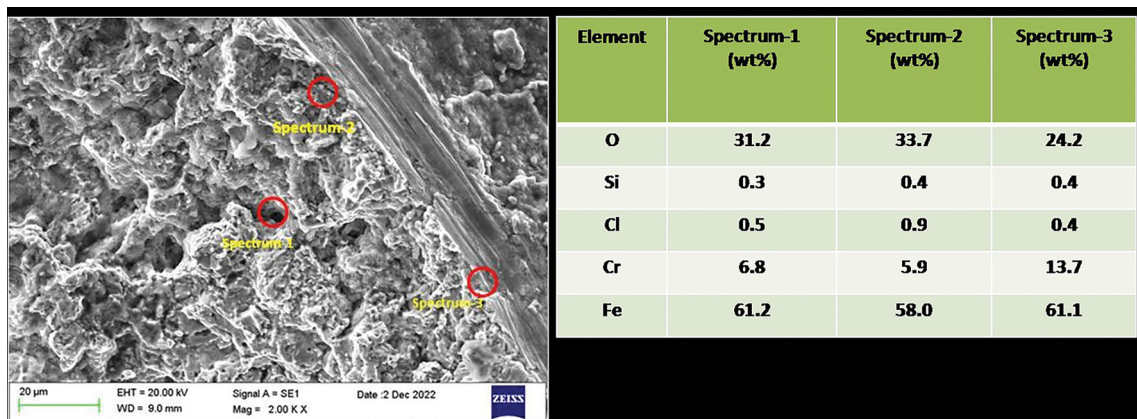


Fig. 5 EDS analysis at pit location of the fracture region

difference between the carbide and matrix. Aggressively chlorinated atmosphere further damages the chromium oxide layer and encourages the pit initiation and growth. Mechanisms of pitting are not well understood yet but the most believed mechanism is that chloride ions adsorb into the oxide layer at high energy locations (scratch, inclusion, carbides) and diffuse to metal/oxide interface. Since enough chromium is not there in the matrix, iron will start sacrificing and form porous brittle oxides. Chlorine reacts with moisture around it and forms an acid environment in

the pit location where further increases the localized attack until it perforates or fails.

Pitting corrosion of martensitic stainless steels is a complex phenomenon. Primary carbides ( $M_7C_3$ ) coming through solidification are more noble than surrounding martensite matrix due to their higher Cr content and lower Fe content. It indicates they have higher corrosion resistance than matrix. The exact potential can vary depending on specific carbide type and its associated composition and environment. Primary carbides like  $M_7C_3$  (Orthorhombic)



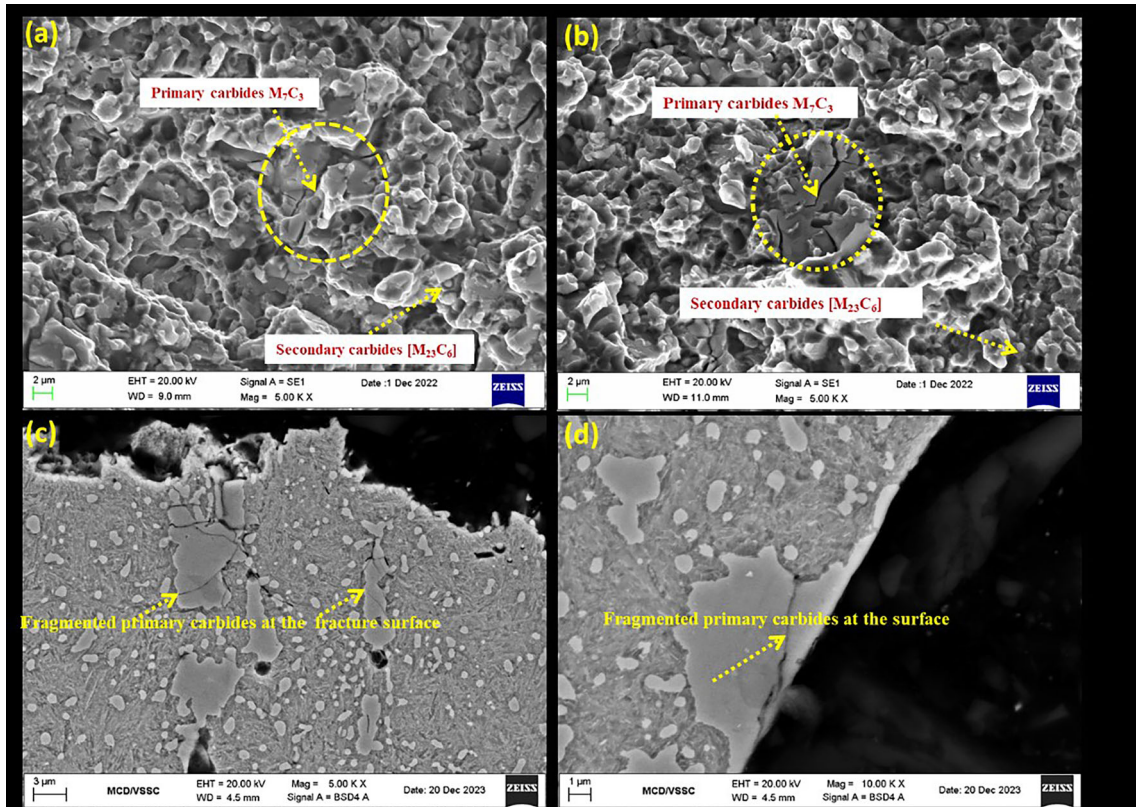


**Fig. 6** SEM Fractographs showing (a, b) Fracture surface and (c, d) Polished surface near to fracture

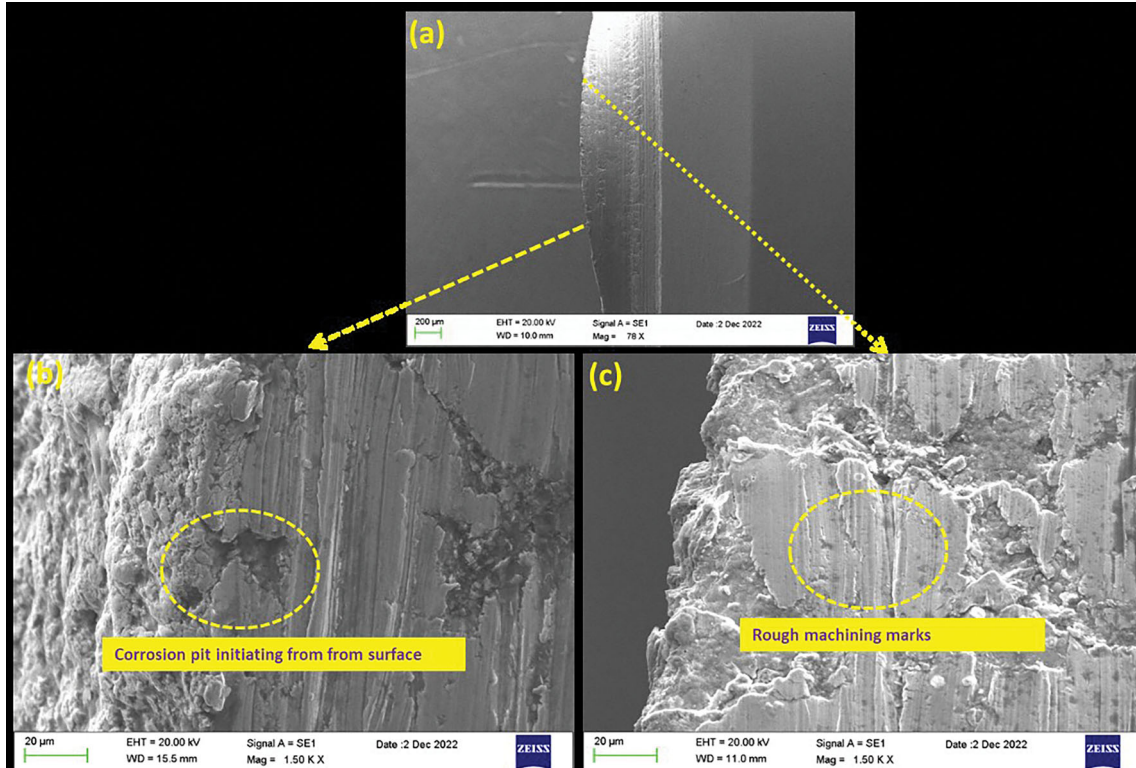


**Fig. 7** SEM Fractographs showing pits and rough machining marks

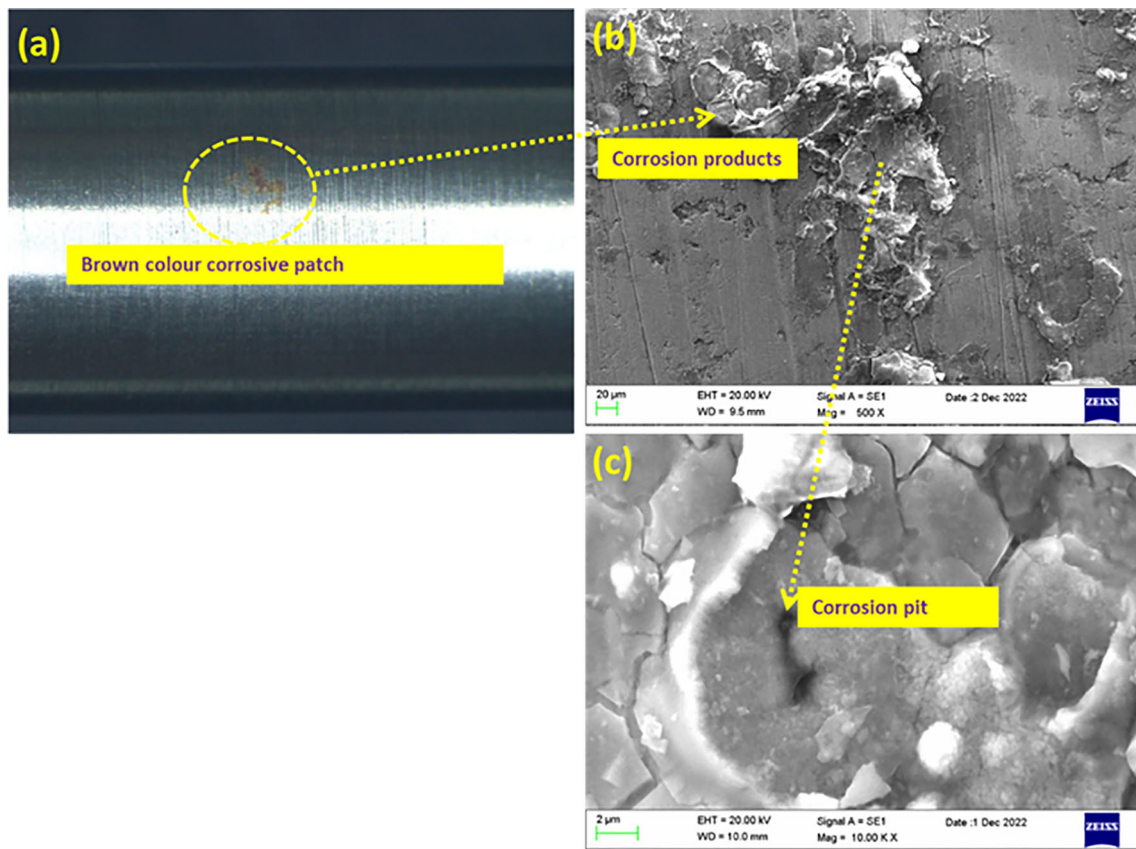


Fig. 8 Pit location away from the fracture edge with corrosion products

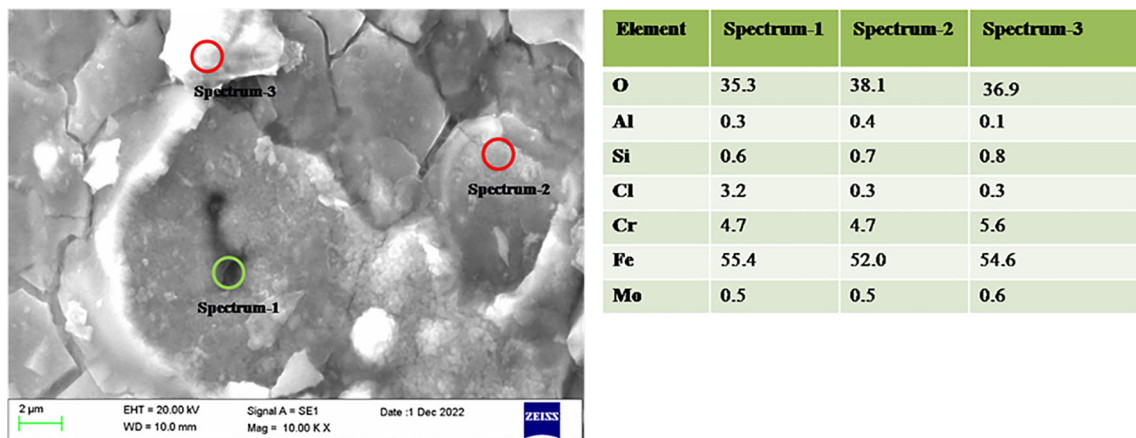


Fig. 9 EDS analysis on the Pit surface and away for pit

and secondary carbides like  $M_{23}C_6$  (FCC) with different Cr/Fe ratios and crystal structures have slight variations in their corrosion potential.

Factors affecting pitting potential

1. Carbide Type and Its Composition

Among primary carbides ( $M_7C_3$ ), secondary carbides ( $M_{23}C_6$ ) and martensitic matrix, primary carbides will have higher Cr/Fe ratio than the rest two. Martensitic

matrix near to primary carbides will have very low Cr/Fe ratio with respect to primary carbide. This will generate a potential difference leading to the initiation of corrosion pits.

2. Heat treatment and Microstructure

Improper austenite treatment and improper tempering can make martensitic matrix with less Cr/Fe. Austenitizing at higher temperature dissolves most of the



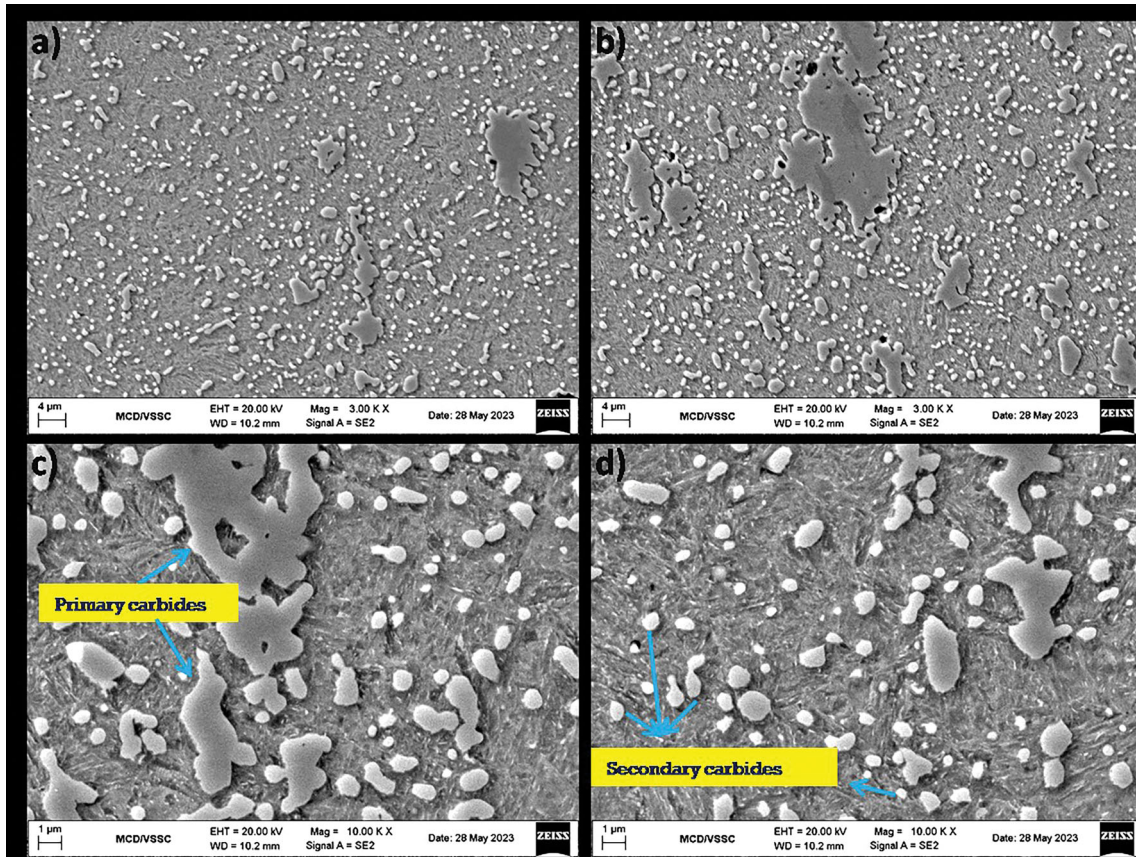
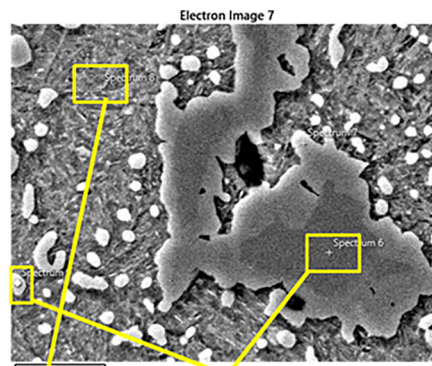


**Fig. 10** SEM micrographs showing the primary and secondary carbides

**Fig. 11** EDS Elemental analysis on the chromium-rich phases and martensitic matrix



Element	Martensitic matrix( Wt%)	Primary carbide( Wt%)	Secondary carbide( Wt%)	Specification, wt.%
C	-	16.1	15.7	1.2 max
Si K	0.5	-	-	1 max
Cr K	15.4	58.1	29.9	16-18
Fe K	83.0	24.3	56.3	balance
Mn K	0.6	0.2	0.4	1 max
Mo L	0.5	1.3	0.7	0.75 max



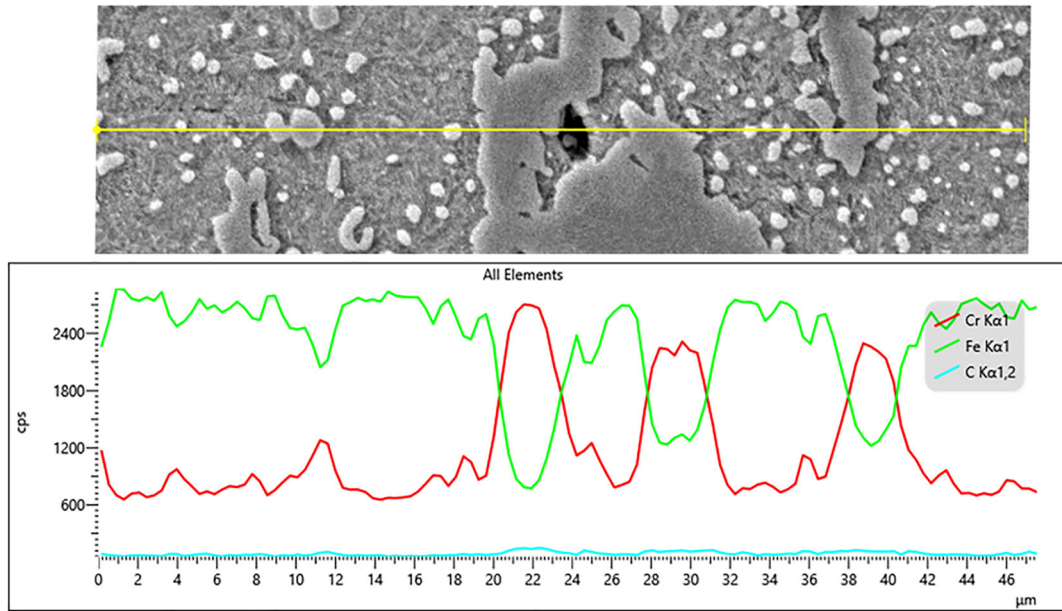


Fig. 12 EDS line scan analysis showing Cr distribution

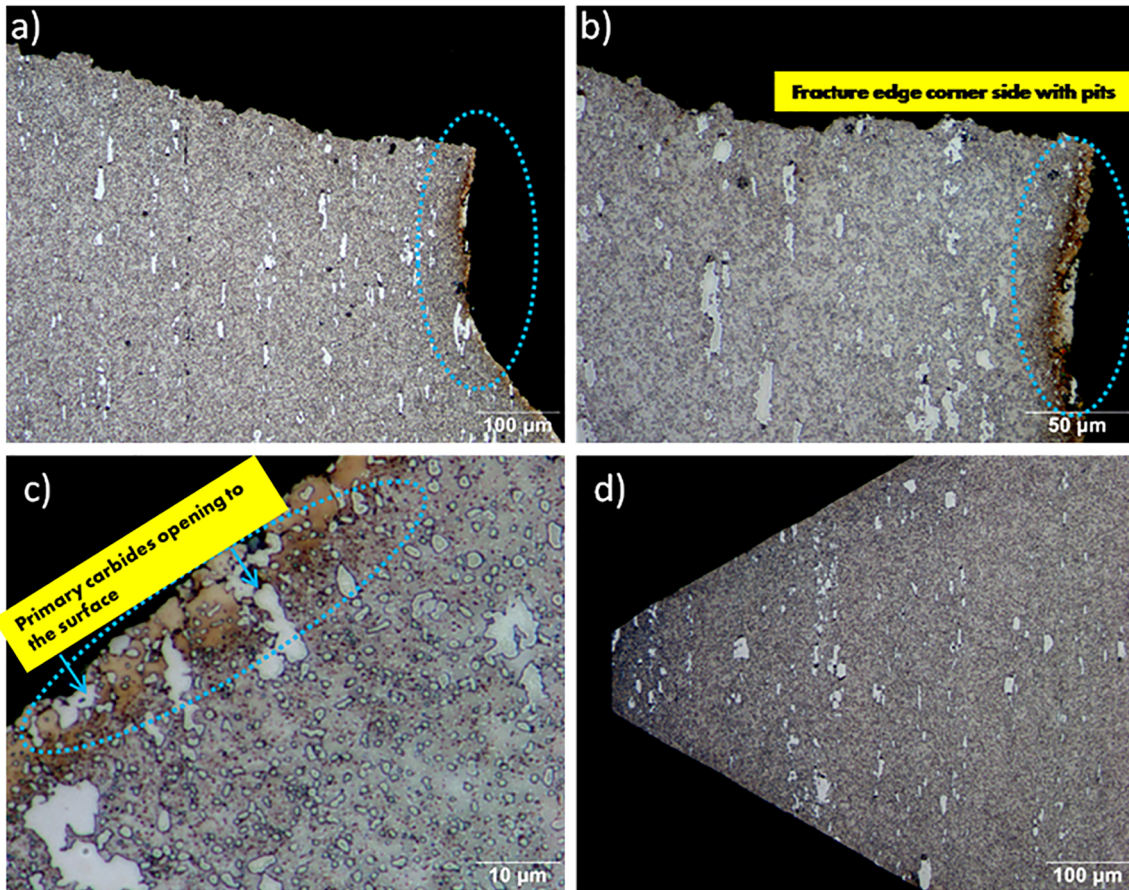
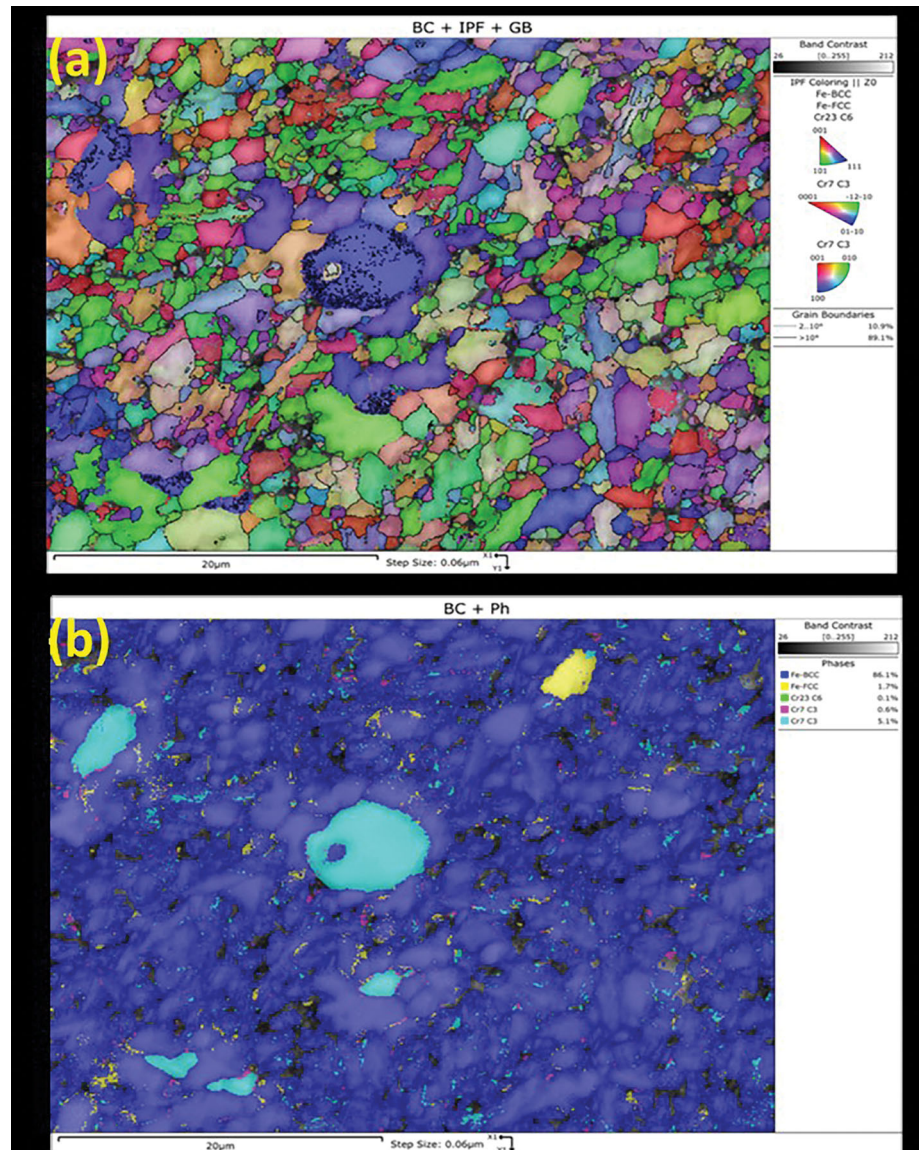


Fig. 13 Optical micrographs of the fracture surface of HAV spool M5 threaded side

**Fig. 14** EBSD maps showing (a) BC + IPF + GB (b) BC + Ph



primary carbides, and matrix enrich with Cr; hence, pitting resistance improves. Tempering at higher temperature also can deplete the chromium content from the matrix through secondary carbide formation [5].

### 3. Electrolyte Composition and pH

The specific environment where the stainless steel is used can significantly impact the pitting potential of both carbides and matrix. Higher concentration and high pH can lead to immediate pitting [4].

### Microscopy and Microhardness

Optical microscopic observations on the polished cross section of M5 threaded region side revealed microstructure

consists of plate martensite, primary and secondary carbides. Most of the primary carbides align perpendicular to the fracture edge. Some of the carbides get fragmented during fracture. No secondary cracks near the fracture edge and corrosion were observed at cross section change location of the HAV spool as shown in Fig. 13a and b. Primary carbides opened to machined surface and pitting corrosion was initiated near to primary carbides (Fig 13c). During the formation of primary carbides, chromium from the matrix is taken, and subsequently, martensite matrix is leaned with elemental chromium. By any chance if the passivated chromium oxide layer gets damaged, pits will nucleate around the primary carbide since there is not enough chromium to heal the damages. Primary carbides opening to the surface during machining will create problem as the carbides are brittle compounds (Fig. 13c).



However, no damage was found in the threads, which were made by machining process (Fig. 13d). Microhardness measurements are in the range of 595–610 VHN.

Pitting corrosion is an extremely localized form of corrosion which ended up with holes in the alloy. These pit holes may be small or big and deep or shallow; it depends on the environment. Deeper pits can create more damage with less weight loss. It is difficult to identify the pitting corrosion at starting stage since pits diameter is in micro-level. It will take time to become visible to the naked eye. Pitting is more dangerous under dynamic loading conditions than static conditions.

EBSD analysis was performed on the specimen away from fracture. BC(Band Contrast) + Ph(Phases) maps have shown the presence of  $M_{23}C_6$ ,  $M_7C_3$  carbides and small fraction of austenite (Fig. 14b). Primary carbides are bigger in size than secondary carbides. BC + IPF + GB map shows plate martensite oriented randomly (Fig. 14a).

### Conclusions and Preventive Actions

Detailed analysis was carried out on the hydraulic amplifier valve spool to understand the root cause of the failure. The failure was observed at the undercut region of the M5 thread side. Fracture surface revealed a pit of approximately 612  $\mu\text{m}$ . Elemental analysis using EDS confirmed the presence of oxygen and chlorine in the pit. Microstructure and microhardness are typical of AISI 440C steel in hardened and tempered condition. The pits were attributed to primary carbides exposed on the machined surface. Ultimately, the failure of the HAV spool was attributed to the corrosion-assisted overload. To avoid future failures related to corrosion in aggressive environments following actions are suggested.

- (a) Regular inspection at inaccessible corners and undercut regions.
- (b) Corrosion protection using lubrication or keeping in oil,
- (c) Alternatives of 440C like CR-30 and 15-5PH can be used.

**Acknowledgments** Authors wish to place on record their deep sense of gratitude to Group Director, Materials and Metallurgy Group and Deputy Director, Materials and Mechanical Entity for their encouragement and support during the course this work. Authors acknowledge Director, VSSC for permission to publish the work.

### References

1. S.C. Krishna, K.T. Tharian, K.V.A. Chakravarthi, A.K. Jha, B. Pant, Heat treatment and thermo-mechanical treatment to modify carbide banding in AISI 440C steel: a case study. *Metallogr. Microstruct. Anal.* **5**, 108–115 (2016). <https://doi.org/10.1007/s13632-016-0266-0>
2. S.K. Manwatkar, A. Bahrudheen, S.B. Tiwari, S.V.S. Narayana Murty, P. Ramesh Narayanan, Failure analysis of AISI 440C steel ball screws used in the actuator system of a satellite launch vehicle. *J. Fail. Anal. Prevent.* **17**(3), 505–512 (2017). <https://doi.org/10.1007/s11668-017-0268-5>
3. K. Jalaja, S.K. Manwatkar, P. Anand, R. Rejith, S.V.S. NarayanaMurty, Metallurgical analysis of surface distress on balls during the operation of AISI 440C ball bearings for satellite applications. *Eng. Fail. Anal.* **124**, 105376 (2021). <https://doi.org/10.1016/j.engfailanal.2021.105376>
4. S. Pahlavan, S. Moazen, I. Taji, K. Saffar, M. Hamrah, M. Moayed, S.M. Beidokhti, Pitting corrosion of martensitic stainless steel in halide bearing solutions. *Corros. Sci.* **112**, 233–240 (2016)
5. A. Barroux, N. Ducommun, E. Nivet, L. Laffont, C. Blanc, Pitting corrosion of 17–4PH stainless steel manufactured by laser beam melting. *Corros. Sci.* **169**, 108594 (2020)
6. J.S. Sheasby, T.L. Walzak, The effect of heat treatment parameters on the anodic polarization behavior of 440C stainless steel. *Corrosion.* **39**(12), 502–507 (1983)
7. J.S. Sheasby, T.L. Walzak, Passivation of 440C stainless steel and the copper sulphate test. In *International Congress on Metallic Corrosion*, Toronto, Canada, 3–7 Jun 1994, pp. 444–448
8. Anon, Steel, corrosion resistant, bars, wire and forgings, 17Cr-0.52 Mo-(0.95 to 1.2 C) (SAE 51440C), consumable electrode vacuum melted. In *Aerospace Material Specification—AMS 5618F*, (SAE International, Warrendale, PA, 2000).
9. T.P. Savas, A.Y.-L. Wang, J.C. Earthman, The effect of heat treatment on the corrosion resistance of 440C stainless steel in 20%  $\text{HNO}_3$  + 2.5%  $\text{Na}_2\text{Cr}_2\text{O}_7$  solution. *J. Mater. Eng. Perform.* **12**(2), 165–171 (2003). <https://doi.org/10.1361/105994903770343303>
10. J.R. Yang, T.H. Yu, C.H. Wang, Martensitic transformations in AISI 440C stainless steel. *Mater. Sci. Eng. A.* **438–440**, 276–280 (2006). <https://doi.org/10.1016/j.msea.2006.02.098>
11. H.K.D.H. Bhadeshia, Steels for bearings. *Prog. Mater. Sci.* **57**, 268–435 (2012). <https://doi.org/10.1016/j.pmatsci.2011.06.002>
12. J.R.J. Marcuci, E.C. De Souza, C.C. Camilo, P.L. Di Lorenzo, J.M.D.A. de Rollo, Corrosion and microstructural characterization of martensitic stainless steels submitted to industrial thermal processes for use in surgical tools. *Rev. Bras. Eng. Biomed.* **30**, 257–264 (2014). <https://doi.org/10.1590/rbeb.2014.025>
13. K. Jalaja, S.K. Manwatkar, R.K. Gupta, S.N. Murty, Metallurgical analysis of failed AISI 440C hydraulic amplifier valve spool for launch vehicle actuators. *J. Fail. Anal. Prevent.* **23**(2), 728–738 (2023). <https://doi.org/10.1007/s11668-023-01597-9>

**Publisher's Note** Springer Nature remains neutral with regard to jurisdictional claims in published maps and institutional affiliations.

Springer Nature or its licensor (e.g. a society or other partner) holds exclusive rights to this article under a publishing agreement with the author(s) or other rightsholder(s); author self-archiving of the accepted manuscript version of this article is solely governed by the terms of such publishing agreement and applicable law.